Planetary and Space Science 68 (2012) 3–17

Contents lists available at ScienceDirect

Planetary and Space Science

journal homepage: www.elsevier.com/locate/pss

Hydrogen peroxide on Mars: Observations, interpretation and future plans

T. Encrenaz [a,*], T.K. Greathouse [b], F. Lefèvre [c], S.K. Atreya [d]

[a] LESIA, Observatoire de Paris, CNRS, UPMC, UPD, France
[b] SWRI, San Antonio, TX, USA
[c] LATMOS/IPSL, CNRS, Paris, France
[d] Department of Atmospheric, Oceanic, and Space Sciences, University of Michigan, Ann Arbor, MI 48109-2143, USA

ARTICLE INFO

Article history:
Received 7 December 2010
Received in revised form
18 March 2011
Accepted 29 March 2011
Available online 15 April 2011

Keywords:
Mars
Mars atmosphere
Mars photochemistry
Infrared spectroscopy

ABSTRACT

Ever since the Viking mass spectrometer failed to detect organics on the surface of Mars in 1976 (Biemann et al., 1976), hydrogen peroxide (H_2O_2) has been suggested as a possible oxidizer of the Martian surface (Oyama and Berdahl, 1977). However, the search for H_2O_2 on Mars was unsuccessful for three decades. In 2003, hydrogen peroxide was finally detected using two ground-based independent techniques, first with submillimeter heterodyne spectroscopy (Clancy et al., 2004) and then again with thermal infrared imaging spectroscopy (Encrenaz et al., 2004). The latter method has been used to simultaneously monitor the abundances and spatial distributions of H_2O_2 and H_2O on Mars as a function of the seasonal cycle. Comparison with the LMD Global Climate Model (GCM) shows that the observations favor simulations taking into account heterogeneous chemistry (Lefèvre et al., 2008). It has been suggested (Delory et al., 2006; Atreya et al., 2006, 2007) that large amounts of hydrogen peroxide could be generated by triboelectricity during dust storms or dust devils. This paper presents a review of the present H_2O_2 dataset and an analysis of observability of peroxide during such events using present and future means.

1. Introduction

Planet Mars shares with the Earth several striking similarities. The two planets have very similar rotation periods and obliquities. Like the Earth, Mars exhibits a seasonal cycle with seasonal polar caps. Unlike the atmosphere of Venus, the atmosphere of Mars is clear so that the planet's surface is visible at optical wavelengths. The surface of Mars shows similarities with terrestrial deserts, large volcanoes, and a vast canyon, Valles Marineris. The apparent similarity between the Earth and Mars has been a major driver for the early space exploration of the red planet.

However, there are two major differences between the two planets. First, at 1.5 AU from the Sun, Mars is more distant and thus colder; its mean surface temperature is about 220 K, or about 60 K lower than the Earth's surface temperature. Second, the planet is smaller, with a mass about one tenth of the terrestrial mass. Its gravity field and its internal energy (generated by the radiogenic elements in its interior) are thus weaker. As a result, the Martian atmosphere, fed both by outgassing and meteoritic impacts, is less dense than in the case of Venus and the Earth; its mean surface pressure is about 6 mbars. In addition, the lower temperature leads to the partial condensation of the major atmospheric molecule, CO_2 so that a third of the atmospheric CO_2 seasonally deposits on the surface in the winter. As a consequence of its low mass, the Martian atmosphere has a very rapid response to changes of solar radiation. A very active Hadley circulation develops over the seasonal cycle, generating dust storms, which can lift particles above 50 km. These large-scale dust storms usually start in the southern hemisphere during southern summer, at the time of perihelion, when the north–south temperature contrast is maximum.

The first step of Martian space exploration was achieved by Mariner 4, which sent back to Earth the first images of the planet's surface that showed no evidence of Percival Lowell's canals but revealed a heavily cratered surface, A few years later, Mariner 9 imaged the entire surface of Mars, including the Tharsis volcanoes and Valles Marineris, and found possible signs of the presence of running liquid water, in the form of valley networks and outflow channels. When and for how long was liquid water present on Mars? Was this period extended enough over time for early life to have appeared and developed? These were pending questions when the Viking mission was launched.

Composed of two orbiters and two landers, the Viking mission carried a comprehensive set of remote sensing and in-situ instruments. Several experiments were devoted to search for living organisms: metabolic experiments, biological experiments, and a gas-chromatograph mass spectrometer to search for organics. No organic compounds were found at either of the two

* Corresponding author. Tel.: +33 1 45 07 76 91; fax: +33 1 45 07 28 06.
E-mail address: therese.encrenaz@obspm.fr (T. Encrenaz).

0032-0633/$ - see front matter © 2011 Elsevier Ltd. All rights reserved.
doi:10.1016/j.pss.2011.03.019

landing sites (Chryse Planitia and Utopia Planitia) with upper limits ranging from 0.0015 parts per billion (ppb, 10^{-9}) for naphthalene to 80 ppb for benzene, with most detection limits smaller than 1 ppb (Biemann et al., 1976; Biemann, 1979). This demonstrated that there is presently no biological or abiological synthesis at these sites, nor any remnant of past biological or abiological processes at these two sites (Klein et al., 1992). In spite of some controversy generated by the interpretation of the biological experiments, it became clear to most of the scientific community that no sign of life had been found on Mars. As a consequence, the interest of the public for the red planet waned and, on the US side, the exploration of Mars was stopped for about two decades. Nevertheless, the Viking mission was an outstanding success, both from a scientific and a technological point of view, and the database collected by the Viking instruments is still used as a reference today.

Over the past decade, there has been a renewal of interest about Mars, its early history and the possible presence of extinct or extant life on the planet. Unlike Venus and the Earth whose surfaces have been re-shaped by volcanism and/or plate tectonics over the past few hundred million to one billion years, Mars has the advantage of keeping the memory of its past history, especially in the ancient, heavily cratered highlands of its southern hemisphere. New discoveries by the orbiters Mars Global Surveyor, Mars Odyssey, Mars Express and Mars Reconnaissance Orbiter, and by the two rovers Spirit and Opportunity, have revealed new information about the early history of Mars including water-ice or permafrost detected at high latitudes, in the first meter of the Martian regolith; an intrinsic magnetic field that was present at the beginning but the dynamo stopped before the end of the first Gy; possible presence of large quantities of liquid water during this period, leading to the formation of phyllosilicates and to sulfates during later episodes. If liquid water was present, the early Martian atmosphere must have been denser and wetter than today. Moreover, the *D*/*H* ratio derived from the Martian water vapor is found to be enriched by a factor 5 relative to the terrestrial Standard Mean Ocean Water value, providing further evidence of wetter Mars in the past. Did life appear during this early period? This key question continues to be the driver of the future exploration of Mars over the coming decade and beyond.

Regarding the Viking results, the unexpected absence of organics at the surface remains to be understood. Indeed, even in the absence of life, organic material is delivered to the Martian surface through meteorites, comets and interplanetary dust particles. In addition, the Gas Exchange Experiment (GEx) revealed the release of oxygen when nutrients and water were added to the soil (Oyama and Berdahl, 1977). Both observations suggest the presence of a powerful oxidizer, and hydrogen peroxide H_2O_2 was proposed as a possible candidate (Oyama and Berdahl, 1977).

Another potential oxidant for the organics on Mars is perchlorates. Perchlorate salts were first detected at the polar landing site of the Phoenix Lander (Hecht et al., 2009). Moreover, recent reanalysis of the Viking GCMS data (Navarro-González et al., in press) indicates that chloromethane and dichloromethane seen in the GCMS data must have been from the surface of Mars, not terrestrial contaminants, contrary to the original reports (Biemann et al., 1976). The new analysis also estimates the abundance of perchlorates in the midlatitude landing site of the two Viking Landers. The chloromethanes result from the action of perchlorates on the organics. Although perchlorates are an ineffiecient oxidizer, their mineral processing in the Martian regolith could result in highly efficient oxidizing agents (Atreya, in press; Atreya et al., 2011). The purported presence of organics and oxidant, perchlorate, in the Viking landing sites still needs to be confirmed by future landed missions such as the Mars Science Laboratory. In this paper we will focus on peroxide, which is known to be an oxidizer of organics.

The presence of H_2O_2 was indeed expected on the basis of photochemical models (Atreya and Gu, 1995; Nair et al., 1994, Krasnopolsky, 1993, 1995). However, the predicted abundance of H_2O_2 in the atmosphere was quite low, a maximum of only a few tens of ppb, far too low to destroy the organics on the surface of Mars. (Hunten, 1979; Huguenin, 1982). From laboratory experiments, Mancinelli (1989) estimated that 20–250 ppm of H_2O_2 would be required to destroy the organics. It is important to note, however, that hydrogen peroxide is known to not destroy simple organic molecules such as methane directly (Wong et al., 2003); it can destroy more complex organic material as confirmed by laboratory experiments (Quinn and Zent, 1999; Gough et al., 2011). On the other hand, mineral processing of peroxide in the surface can lead to highly reactive hydroperoxy and hydroxyl radicals as well as superoxides that could destroy all organics including methane very efficiently (Atreya, in press; Atreya et al., 2011).

It took a long time for observers to detect hydrogen peroxide. Bjoraker et al. (1987), using a cooled grating combined with an FTS at the Kitt Peak solar telescope, derived an upper limit of a few hundreds of ppb in October 1986, ten years after the Viking mission. This upper limit was improved upon by Krasnopolsky et al. (1997) who inferred an upper limit of 30 ppb in June 1988, using the Goddard post-disperser with the Kitt Peak FTS. Finally Encrenaz et al. (2002) derived a stringent upper limit of 10 ppb from observations made with the TEXES high resolution imaging spectrometer at IRTF, which was barely compatible with photochemical models.

The detection of hydrogen peroxide on Mars was finally achieved in 2003 using two independent measurements, both performed from the ground. Clancy et al. (2004) first reported the H_2O_2 detection with a disk average mixing ratio of 18 ppb from their submillimeter heterodyne spectroscopy observations performed in September 2003. One month later, Encrenaz et al. (2004) reported the detection and mapping of H_2O_2 using the TEXES instrument at the IRTF in June 2003. The H_2O_2 mixing ratio was found to range between 20 and 40 ppb. The observed H_2O_2 mixing ratios from both datasets were well in agreement with photochemical models, indicating significant variations over the seasonal cycle. Since 2003, the Martian hydrogen peroxide has been regularly monitored using TEXES at the IRTF. Water vapor maps have been simultaneously retrieved using weak HDO transitions in the vicinity of the H_2O_2 lines. Both datasets have been compared with simulations by the Global Climate Model developed at LMD-Oxford (Forget et al., 1999, 2006; Lefèvre et al., 2008).

In this paper we first review the H_2O_2 and H_2O datasets that have been recorded with the TEXES instrument since 2002. Over the same period, the development of GCMs with photochemistry (Lefèvre et al., 2004; Moudden, 2007) has allowed to predict the spatial and seasonal variations of minor chemical species over the Martian disk. In this paper, each TEXES observation has been compared with the simulations of the LMD Global Climate Model with coupled photochemistry (Forget et al., 1999; Lefèvre et al., 2008). As will be shown, the TEXES measurements favor simulations including heterogeneous chemistry, rather than pure gas-phase models. In a second part of the paper, the hypothesis of an additional electrochemical source of H_2O_2 source (Delory et al., 2006; Atreya et al., 2006, 2007) is reviewed briefly, followed by a discussion of possible observational means for detecting such events with present and future facilities.

2. The hydrogen peroxide molecule

2.1. Formation and destruction of hydrogen peroxide on Mars

One-dimensional, globally averaged photochemical models have all predicted the formation of a small amount of H_2O_2 in

the Martian atmosphere (Parkinson and Hunten, 1972; Krasnopolsky, 1986, 1993, 1995; Atreya and Gu, 1995; Nair et al., 1994; Clancy and Nair, 1996). According to these models and the current consensus on photochemistry, H_2O_2 is formed by the self-reaction of the HO_2 radicals produced by the H_2O photolysis:

$$H_2O + h\nu \rightarrow OH + H$$

$$OH + CO \rightarrow H + CO_2$$

$$H + O_2 + CO_2 \rightarrow HO_2 + CO_2$$

$$HO_2 + HO_2 \rightarrow H_2O_2 + O_2$$

Hydrogen peroxide is mainly destroyed through its dissociation into OH:

$$H_2O_2 + h\nu \rightarrow 2OH$$

The photolysis of H_2O_2 is relatively fast and leads to a photochemical lifetime of about 6 h during the day. However, once photodissociated, H_2O_2 is rapidly reformed from its photolysis products. As a result, the predicted abundance of H_2O_2 on Mars shows only a small diurnal variability (Fig. 1). At night, H_2O_2 has no significant loss process and behaves like a passive tracer transported by the winds. Under particularly cold conditions, H_2O_2 condensation may occur near the surface at night, as suggested by GCM simulations (Moudden, 2007).

Because HO_2 radicals (the source of H_2O_2) are secondary products of the dissociation of H_2O, photochemical models predict a tight correlation between the H_2O and H_2O_2 abundances. This can be seen from the H_2O_2 vertical distribution, which mimics that of H_2O and shows the same orbital variability (Fig. 1). Similar to H_2O, H_2O_2 is essentially confined near the Martian surface and its mixing ratio drops rapidly above the hygropause. The vertical extent of the H_2O_2 layer also follows the large vertical excursion of the hygropause from the cold aphelion conditions to the warmer perihelion season (Clancy and Nair, 1996).

The above photochemical models have been developed under the assumption of homogeneous gas-phase chemistry only. By analogy with the terrestrial atmosphere, where reactions on clouds play a key role in the chemistry of polar ozone, Krasnopolsky (2006) and Lefèvre et al. (2008) have introduced heterogeneous reactions on ice clouds in their photochemical models. It has been shown that, in the case of both ozone and hydrogen peroxide, the agreement between observations and models is significantly improved when heterogeneous chemistry is taken into account (Lefèvre et al. 2008).

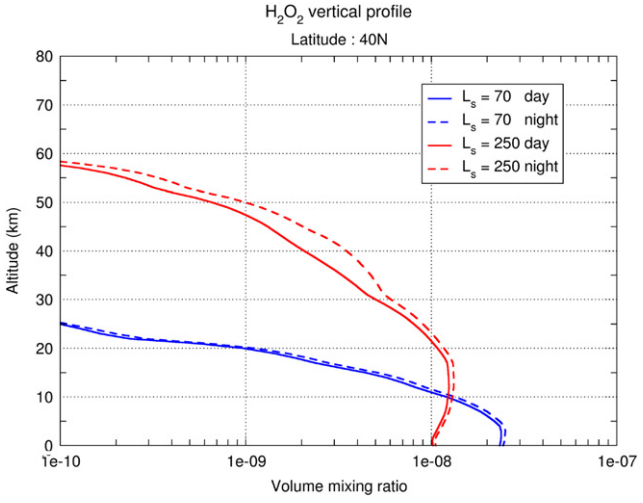

Fig. 1. Examples of vertical profiles of H_2O_2 calculated at 40°N for Ls=70° and Ls=250° by the LMD global climate model (Lefèvre et al., 2004). Solid and dashed curves indicate the profile at noon and midnight, respectively.

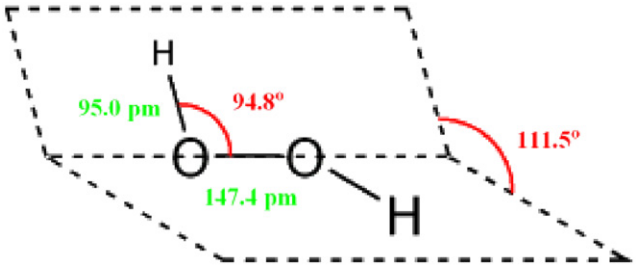

Fig. 2. The structure of the H_2O_2 molecule in the gaseous phase.

2.2. The spectrum of hydrogen peroxide

Hydrogen peroxide, a non-planar molecule of A electronic state and C_2 symmetry group (Fig. 2) with a dipole moment of 2.26 D, has a rich spectrum, which extends from the radio range up to the UV. The molecule has strong rotational transitions at millimeter and submillimeter wavelengths, and six fundamental vibrational bands, which lie in the infrared range: ν_4, centered at 317 cm^{-1} i.e. around 30 μm; ν_3, centered at 863 cm^{-1} (12 μm); ν_6, centered at 1266 cm^{-1} (8 μm) and ν_2, centered at 1393 cm^{-1} (7 μm); ν_1 and ν_5 at 3608 cm^{-1} (2.8 μm). The ν_2 and ν_3 bands are very weak. The ν_4 band is not observable from the ground. The ν_1 and ν_5 bands at 2.8 μm fall within H_2O and CO_2 bands and cannot be used for the study of Mars.

In contrast, the strong ν_6 band around 8 μm, observable from the ground (between the telluric absorptions, mostly due to H_2O and CH_4), is well separated from other Martian species. The only other Martian lines observed in this region are isotopic bands of CO_2 and HDO. With respect to millimeter and submillimeter transitions, which can be observed from the ground at high spectral resolution with heterodyne spectroscopy, imaging spectroscopy in the thermal infrared offers the double advantage of high spatial and spectral resolution.

3. The TEXES data set

3.1. The TEXES instrument: observing strategy

TEXES (Texas Echelon Cross Echelle Spectrograph) is a mid-infrared (5–25 μm) spectrograph with several operating modes: high resolution, cross-dispersed with a resolving power of $R=\lambda/\delta\lambda \sim 100{,}000$, 0.5% spectral coverage, and a $\sim 1.5'' \times 8''$ slit; medium resolution, long-slit with $R \sim 15{,}000$, 0.5% coverage, and a $\sim 1.5'' \times 45''$ slit; low-resolution, long-slit with $\delta\lambda \sim 0.004$ μm, 0.25 μm coverage, and a $\sim 1.5'' \times 45''$ slit; and source acquisition imaging with 0.33″ pixels and a $25'' \times 25''$ field of view on a 3-m telescope (Lacy et al. 2002). TEXES has been used at the McDonald Observatory 2.7-m and the NASA Infrared Telescope Facility 3-m telescopes, and more recently on the GEMINI-N 8-m telescope.

We have been using TEXES at IRTF since 2001 in a long-term observing program for detecting and monitoring hydrogen peroxide on Mars. We have used the high-resolution mode in a series of spectral intervals ranging from 1226 to 1243 cm^{-1}. Table 1 summarizes the observations.

Using a 1.1×8 arcsec slit, aligned with the celestial N–S axis, we stepped the telescope east by 0.5 arcsec between two successive 2-s integrations, in order to map the entire Martian disk from west to east. Generally 4 such scans were taken in succession as a

Table 1
Observations of H_2O_2 with TEXES.

Date	Ls (°)	Diameter (″)	Doppler shift (cm^{-1})	Spectral range (cm^{-1})	Observed molecules
Feb. 1–3, 2001	112	6	+0.072	1227–1235	CO_2, HDO
June,19–20,2003	206	15	+0.045	1230–12361237–1244	CO_2, H_2O_2, HDO
Nov 30–Dec 1, 2005	332	17	−0.038	1236–1243	CO_2, H_2O_2, HDO
May 30–June 3, 2008	80	5	−0.058	1232–12371238–1244	CO_2, H_2O_2, HDO
Oct. 11–15, 2009	352	6	+0.051	1232–21371237–1244	CO_2, H_2O_2, HDO

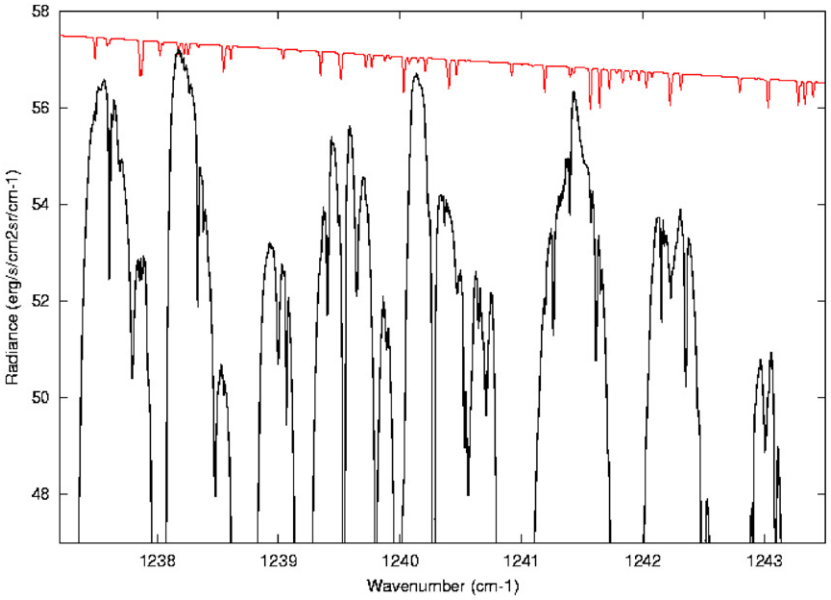

Fig. 3. The spectrum of Mars between 1237.2 and 1243.5 cm^{-1}, integrated over a selected area around of high continuum in the 2003 data set. The synthetic spectrum of H_2O_2 (red curve) corresponds to a mixing ratio of 40 ppb. The strongest absorption lines are due to telluric methane and water lines. The figure is taken from Encrenaz et al. (2004). (For interpretation of the references to color in this figure legend, the reader is referred to the web version of this article.)

single observation file. In the case of the 2003 and 2005 runs, when the diameter was larger than 7 arcsec, we mapped successively the northern and southern hemispheres. The pixel size along the slit length was 0.33 arcsec and the spatial resolution, after binning, was about 1 arcsec. The typical observing time for a set of 4 W–E scans was about 10 min. Observations were co-added over a total of 3–4 h. Images were centered with respect to the limb position and the maximum brightness.

For calibrating the TEXES data, we used a radiometric method commonly used for millimeter and submillimeter observations (Rohlfs and Wilson, 2004). Calibration frames consisting of 2 measurements (black chopper blade and sky) are systematically taken before each observing sequence, and the difference (black-sky) is taken as a flat field (Lacy et al., 2002).

3.2. Line transitions

Numerous H_2O_2 line transitions are present in the 1227–1245 cm^{-1} spectral region. Two doublets are especially strong, the first one at 1234.05 and 1234.10 cm^{-1} (to be compared with a weak CO_2 transition at 1233.975 cm^{-1}) and the second one at 1241.575 and 1241.650 cm^{-1} (to be compared with the 1241.615 cm^{-1} CO_2 transition). It is important to observe a doublet transition to secure the detection, and to use a nearby CO_2 transition to derive an H_2O_2 mixing ratio.

Half a dozen of H_2O_2 transitions were identified in the 2003 data set (Encrenaz et al., 2004; see Fig. 3), including the two doublets mentioned above. In 2001, our upper limit was derived from the combination of six transitions including the 1234 cm^{-1} doublet. In all other cases, both the 1234 cm^{-1} doublet and the 1241 cm^{-1} doublet were used. After 2003, the 1241 cm^{-1} doublet, slightly stronger than the other one, was selected as a H_2O_2 tracer.

A few weak HDO transitions are found in the 1227–1245 cm^{-1} spectral range. We have used the 1226.95 cm^{-1} transition (associated with the 1226.8 cm^{-1} CO_2 line) in 2001; the HDO 1236.295 cm^{-1} transition (associated with CO_2 at 1235.67 cm^{-1}) in 2005 and 2008; the HDO 1239.95 cm^{-1} line (associated with CO_2 at 1241.615 cm^{-1}) in 2003 and 2010. The choice of the transitions was made according to the Doppler shift, in order to avoid contamination by the terrestrial atmosphere.

3.3. Data interpretation and modeling

Maps of the continuum radiance and H_2O_2, HDO and CO_2 line depths were extracted from the data cubes. The continuum map was used to identify the region of maximum radiance and a mean spectrum was integrated over this region to get the best *S*/*N* ratio. This mean spectrum was compared to synthetic spectra calculated using atmospheric parameters extracted from the LMD GCM, under the conditions of observations (Forget et al., 1999). Spectroscopic data were taken from the GEISA data bank (Jacquinet-Husson et al., 2005); in addition, spectroscopic parameters of weak CO_2 isotopic lines, not included in the GEISA linelist, were calculated using the analysis of Rothman (1986).

A mean H_2O_2 mixing ratio over the region of maximum flux was inferred from this comparison.

In order to estimate a H_2O_2 (or HDO) mixing ratio over the Martian disk, we simply ratio the H_2O_2 (or HDO) line depth (averaged from the two doublet components) with the CO_2 line depth ratio. This first-order method has the advantage of minimizing the uncertainties associated with surface and atmospheric properties, including topography, atmospheric and surface temperatures, dust opacity and airmass factor. Synthetic calculations have shown that the retrieved mixing ratio remains constant, typically within 10%, over a wide range of atmospheric parameters. The error may increase, however, up to 25% when the airmass increases, i.e. near the limb (Encrenaz et al., 2008).

In the case of HDO, another uncertainty comes from the *D*/*H* ratio. We have assumed a constant HDO/H_2O mixing ratio of 5 times the terrestrial value, as derived by Krasnopolsky et al. (1997). However, the uncertainty on this determination is 40%. In addition, this assumption may be incorrect, as fractionation effects are expected to be associated to water condensation and sublimation, leading to a change in the *D*/*H* ratio (Fouchet and Lellouch, 2000). Simultaneous observations of HDO and H_2O have been performed by Mumma et al. (2003) and Novak et al. (2007). Montmessin et al. (2005) have calculated the expected *D*/*H* ratio as a function of latitude and seasonal cycle. Their analysis shows that, at low latitudes, the *D*/*H* ratio is close to 5.0 times the terrestrial value. They also indicate lower values toward high latitudes. If this effect is confirmed, our determinations of the water vapor mixing ratio might be underestimated in these regions. These calculations, however, do not agree with the observations of Mumma et al. (2003) and Novak et al. (2007), and a better determination of the *D*/*H* ratio and how it varies on Mars is still needed.

4. Results and interpretation

Results are presented for three different seasons: (1) Northern autumn (Ls=206°, June 2003); (2) Northern summer solstice (Ls=80°, June 2008 and Ls=112°, February 2001); (3) Equinox (Ls=332°, December 2005 and Ls=352°, October 2009).

4.1. Northern autumn (Ls=206°, June 2003)

This data set corresponds to the season for which a maximum H_2O_2 abundance was observed. The surface temperature was high (above 300 K east of the subsolar point), which allowed a very high *S*/*N* ratio (above 1000 in the continuum for the spectrum integrated over the region of maximum radiance). All spectral features with depths down to 0.3%, either Martian or telluric, were identified between 1230 and 1244 cm^{-1}. Fig. 4 shows the best H_2O_2 fit obtained from the 1241 cm^{-1} doublet in the region of maximum radiance, which corresponds to an H_2O_2 mixing ratio of 40 ppb; the same value was inferred from 1234 cm^{-1} doublet.

Water vapor was retrieved from the 1239.95 cm^{-1} HDO transition. The best fit, in the region of maximum radiance, was obtained for an H_2O mixing ratio of 300 ppm (Fig. 5). The surface temperature was inferred from the continuum measurements at 4 different frequencies.

Fig. 6 shows a comparison between TEXES data and the LMD GCM or the H_2O_2 mixing ratio, the H_2O mixing ratio and the surface temperature. It can be seen that the overall agreement is good, both for the absolute scales and the spatial distributions. For the surface brighness temperature map, the discrepancy between TEXES data and the model at high southern latitudes is due to a blurring of the observed image due to pointing uncertainties and/or poor seeing.

4.2. Northern summer solstice

Two datasets were obtained, before and after northern summer solstice (Ls=80°, June 2008 and Ls=112°, February 2001). In both cases, high water content was observed in the northern hemisphere, as expected from models and from previous Viking and TES observations. In contrast, the H_2O_2 mixing ratio was lower than expected from photochemical models assuming only gas-phase chemistry.

4.2.1. Ls=80° (June 2008)

With a maximum surface temperature of 245 K, the *S*/*N* ratio of the data was lower than in the previous set. In addition, the diameter of Mars was only 5 arcsec, which severely limited the

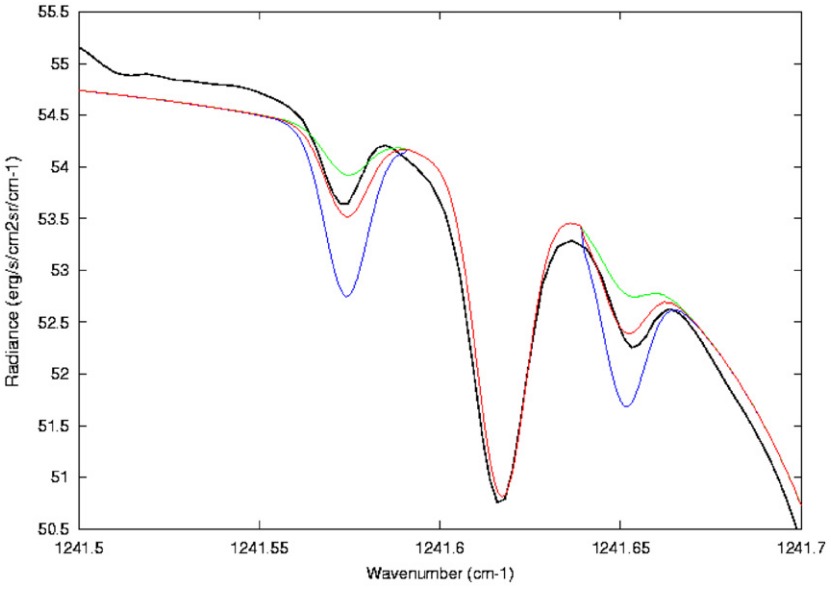

Fig. 4. The spectrum of H_2O_2 in the selected area of high continuum (same as Fig. 3). The two lines of the H_2O_2 doublet bracket a CO_2 transition. Models: 20 ppb (green), 40 ppb (red) and 80 ppb (blue). The best fit is obtained for a mixing ratio of 40 ppb. The figure is taken from Encrenaz et al. (2004). (For interpretation of the references to color in this figure legend, the reader is referred to the web version of this article.)

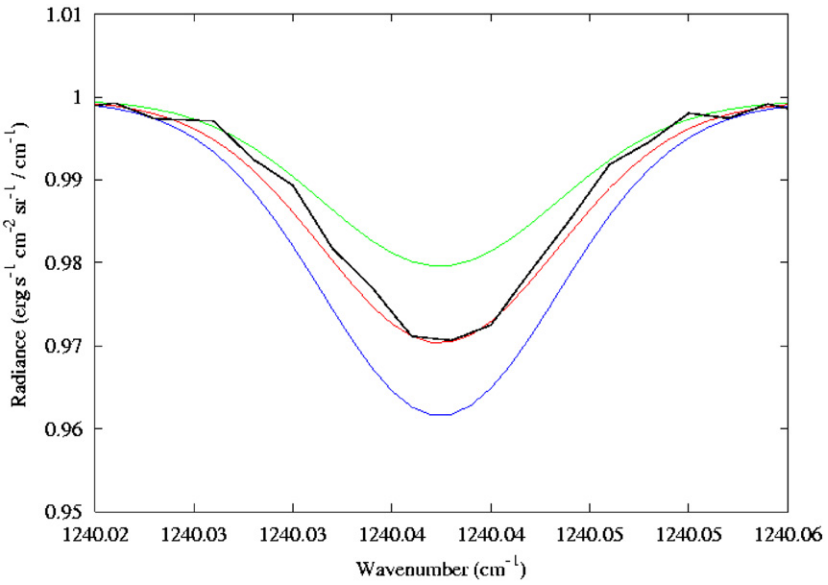

Fig. 5. The HDO Martian line observed in the 2003 data set in the subsolar spectrum of Mars (same region as Figs. 3 and 4. Models: 200 ppm (green), 300 ppm (red), 400 ppm (blue). The D/H ratio in Mars is assumed to be 5 times the terrestrial value. The figure is taken from Encrenaz et al. (2005). (For interpretation of the references to color in this figure legend, the reader is referred to the web version of this article.)

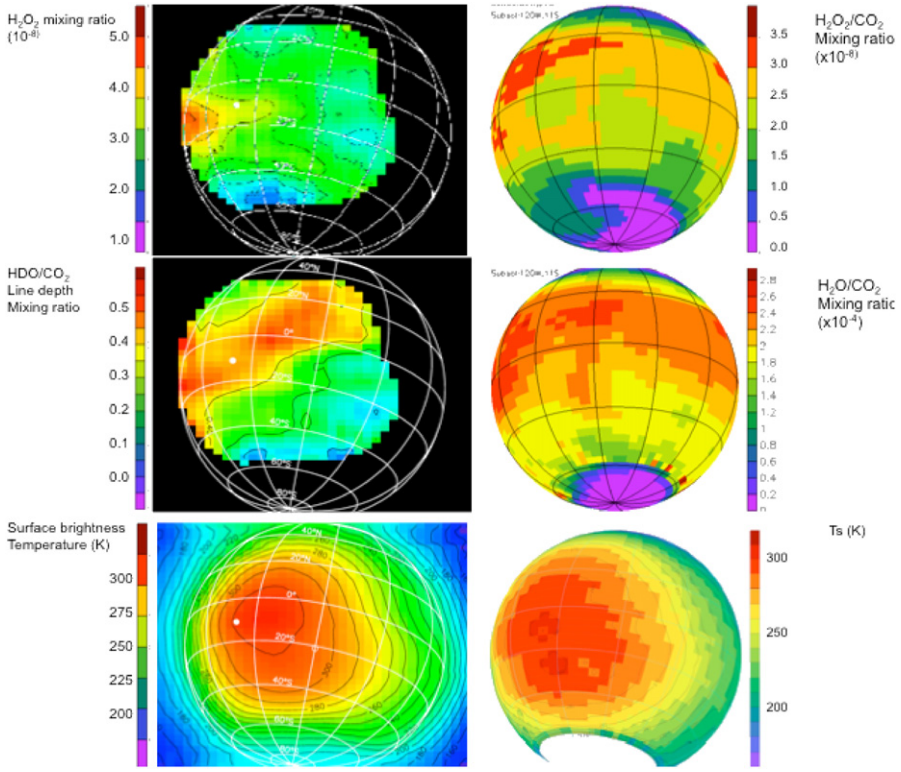

Fig. 6. Comparison of TEXES maps (left) and the LMD GCM calculations (right) for the June 2003 data set (Ls=206°). Top: H_2O_2 mixing ratio (maximum values: 40 ppb). Middle: HDO/CO_2 line depth ratio (left) and H_2O mixing ratio (right). A line depth ratio of 0.5 corresponds to a mixing ratio of 300 ppm. Bottom: Surface temperatures (maximum values: 310 K). The SSP is indicated by a white dot. The figure is adapted from Encrenaz et al. (2004, 2005).

quality of the map. The H_2O_2 transitions were too weak to allow mapping; still, it was possible to obtain a marginal detection of H_2O_2, corresponding to a mixing ratio of 10 ppb, by integrating over the whole disk. This value is weaker than the GCM simulation, which predicts a strong dichotomy between the northern and the southern hemispheres, as expected from the H_2O distribution at this season. The maximum H_2O_2 value calculated by the model is above 20 ppb at high northern latitudes (Fig. 7). It is surprising to see that the TEXES spectra, integrated separately over the northern and southern hemispheres, show no evidence for an increase in the northern side, with a mean mixing ratio of 10 ppb for both hemispheres.

The water vapor mixing ratio was inferred from the 1236.295 cm-1 transition, compared with the 1235.67 cm^{-1} line of CO_2. Fig. 8 shows the best fit achieved for a latitude of 40N, which corresponds to 250 ppm.

Fig. 9 shows a comparison of the maps of the water vapor mixing ratio and the surface temperature obtained with TEXES

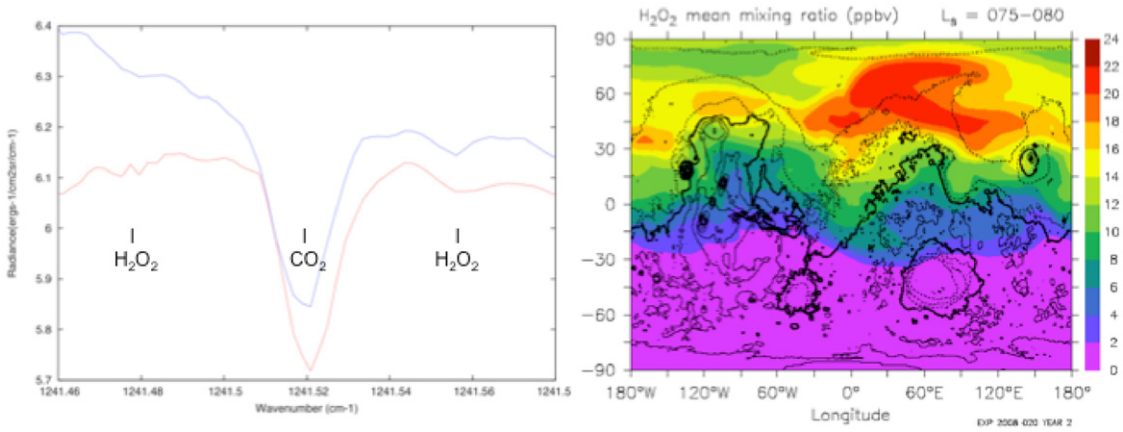

Fig. 7. Left: TEXES spectra integrated over the northern hemisphere (red) and the southern hemisphere (blue). Right: GCM map of H_2O_2 for Ls=80°. There is no evidence in the data for the H_2O_2 enhancement predicted by the GCM in the northern hemisphere. (For interpretation of the references to color in this figure legend, the reader is referred to the web version of this article.)

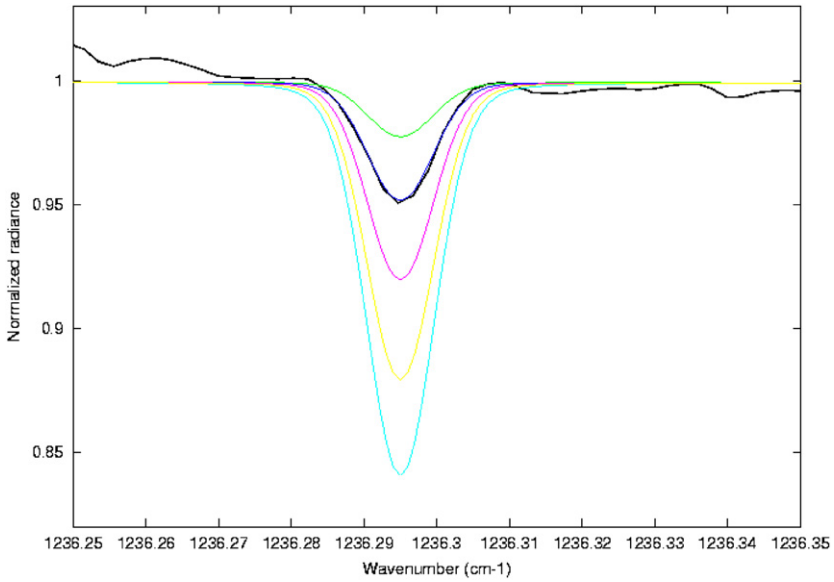

Fig. 8. The TEXES HDO line observed in the 2008 Martian spectrum integrated over 30N and 50N. Models, from top to bottom: H_2O mixing ratios of 100, 250, 500, 750 and 1000 ppm. The best fit is obtained for $[H_2O]$=250 ppm. The figure is taken from Encrenaz et al. (2010).

and predicted by the GCM. It can be seen that in the case of water vapor, the agreement is very satisfactory. It is interesting to notice the slight increase of the H_2O mixing ratio from west to east, i.e. from morning to evening. This trend is also observed in the GCM map. As the GCM is calculated on the basis of dynamical effects associated, in particular, with topography, the good agreement implies that, at northern latitudes lower than 60N, there is no need for any mechanism like regolith desorption to account for the data.

The comparison between the TEXES and GCM surface temperature maps is very puzzling. The TEXES maximum (which corresponds to Elyseum) is in good agreement with the GCM prediction, but the GCM predicts a strong maximum on the evening limb, which is not observed at all on the TEXES data. The origin of this discrepancy is not clear. A possible explanation might be the blurring effect, reinforced, in the case of the 2008 dataset, by the small size of the planet and the poor seeing, as observations took place between 17:00 and 18:00 local time. Thus, in this specific case, the TEXES continuum map is probably not a reliable indicator of the surface temperature.

4.2.2. *Ls=112° (February 2001)*

This short session corresponds to our first attempt to detect H_2O_2 on Mars. The period was thought to be optimized because it corresponded to the maximum amount of water vapor, just after summer solstice. For this reason, maps of the Martian disk were recorded at high northern latitudes. Still, stringent upper limits were obtained over the northern hemisphere and at high northern latitudes, with a mean upper limit of 10 ppb. The observed water vapor content was very high near the northern pole, as expected from previous TES observations. Fig. 10 shows maps of the continuum and the H_2O mixing ratio at high northern latitudes inferred from the ratio of the 1226.95 cm^{-1} HDO line depth to the 1226.81 cm^{-1} CO_2 line depth.

Estimates of the water vapor have been retrieved in two areas, at 40N latitude (morning limb) and in the maximum spot at 70N (Fig. 10). At 40N, the best fit is obtained for $[H_2O]$=250 ppm (i.e. about 15 pr-μm; Fig. 11), in good agreement with GCM predictions and earlier measurements. At 70N, the inferred H_2O content is very high ($>$1000 ppm, i.e. $>$70 pr-μm; Fig. 11). This high value, measured in a local point close to the polar cap, probably corresponds to a specific water outgassing phenomenon.

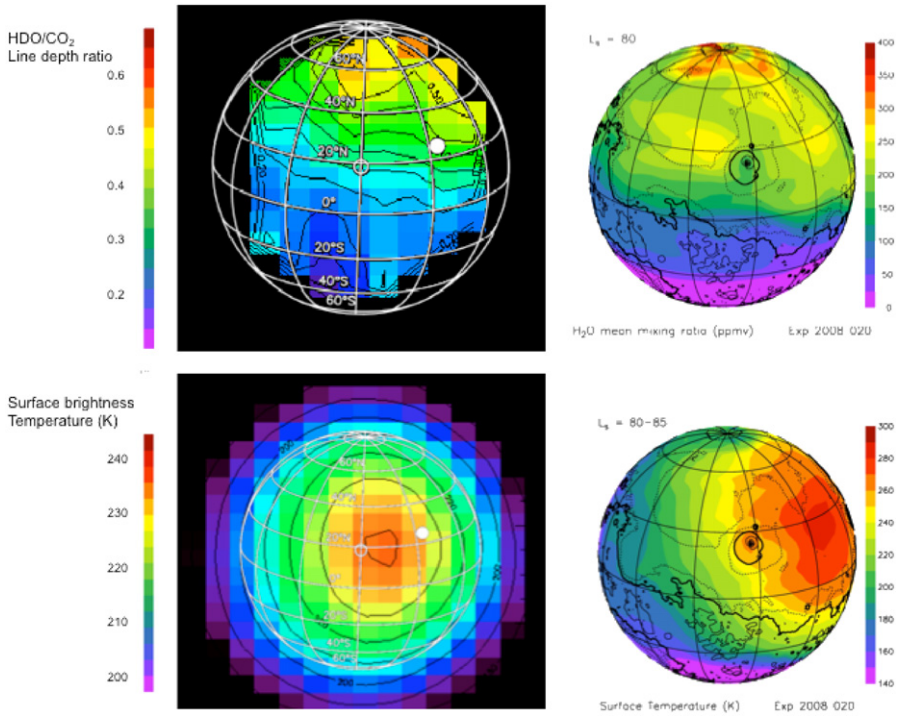

Fig. 9. Comparison of TEXES maps and GCM simulations for the June 2008 data set (Ls=80°). Top: HDO/CO_2 line depth ratio (left) and H_2O mixing ratio (250 ppm at 30N–50N); a line depth ratio of 0.5 corresponds to a water vapor mixing ratio of 250 ppm. Bottom: Surface temperatures (maximum values: 245 K). The SSP is indicated by a white dot. The figure is adapted from Encrenaz et al. (2010).

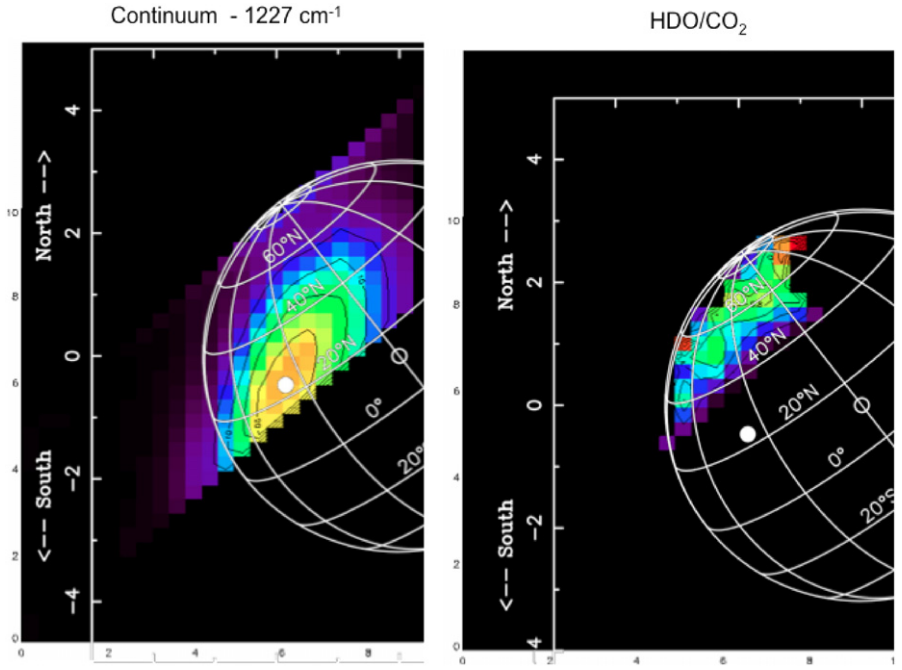

Fig. 10. Left: Continuum map of the Martian northern hemisphere for Ls=112°; the maximum flux is 23 erg/s/cm2sr/cm^{-1}, which corresponds to a brightness temperature of 265 K, assuming an emissivity of 0.95. Right: HDO/CO_2 line depth ratio at high northern latitudes; a line depth ratio of 0.25 (40N, dark blue) corresponds to a H_2O mixing ratio of 250 ppm (see Fig. 11). A ratio of 0.75 (60N, green) corresponds to a mixing ratio of 750 ppm. The white spot corresponds to the subsolar point. (For interpretation of the references to color in this figure legend, the reader is referred to the web version of this article.)

The low abundance of H_2O_2 associated to the large water vapor content for Ls=112° apparently contradicts the expected correlation between the two molecules. As pointed out by Clancy et al. (2004) and Encrenaz et al. (2004), the 2001 observations were done very close to aphelion. As an effect of the low atmospheric temperatures, the water condensation level was probably lower than 10 km (Clancy and Nair, 1996; Encrenaz et al., 2002), and may have resulted in an inhibition of the H_2O_2 photochemical production mechanism.

4.3. Equinox

Two datasets were recorded around equinox, at Ls=332° (December 2005) and Ls=352° (October 2009). In both cases,

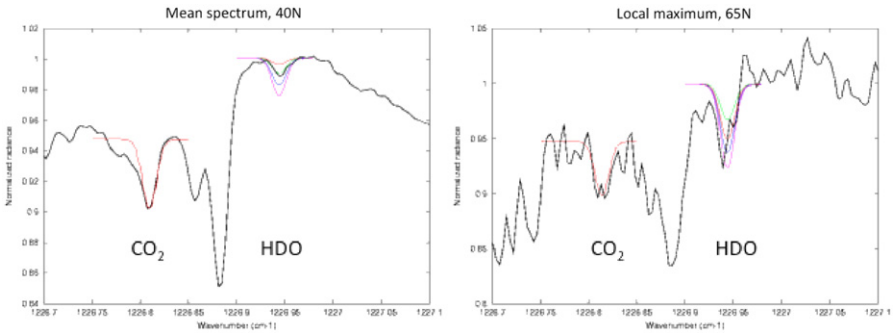

Fig. 11. The spectrum of HDO observed for Ls=112°. Left: Latitude 40N (morning limb). Models: from top to botton, [H_2O]=100, 250, 500, 750 ppm. Right: 70N (maximum point). Models: from top to bottom: [H_2O]=1000, 2000, 3000, 5000 ppm. The poor *S/N* seriously limits the fit quality in the case of the 70N spectrum.

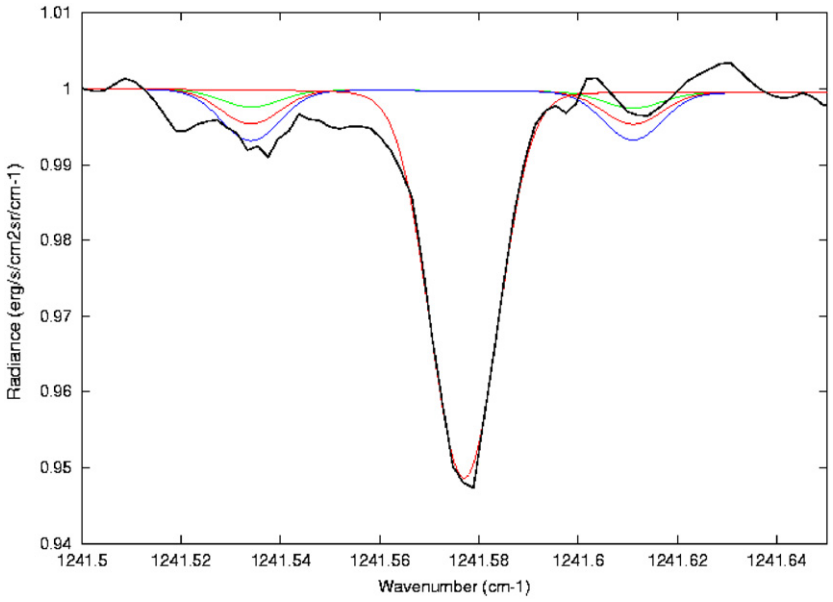

Fig. 12. The TEXES spectrum of H_2O_2, observed in December 2005 (Ls=332°), averaged over an area close to the southern evening limb, corrected from the continuum slope and compared with synthetic models. Green: 10 ppb; red: 15 ppb; blue: 20 ppb. The figure is taken from Encrenaz et al. (2008). (For interpretation of the references to color in this figure legend, the reader is referred to the web version of this article.)

the inferred H_2O and H_2O_2 abundances were found to be lower than predicted by the LMD GCM. However, as discussed below, a recently revised version of the GCM, including a slightly lower water vapor content, is now able to fit the H_2O_2 observations around equinox (see Sections 4.3.2 and 5.1, and Fig. 16). Some discrepancies were also observed in the spatial distributions of H_2O_2 and water vapor.

4.3.1. *Ls=332° (December 2005)*

Fig. 12 shows the mean spectrum of H_2O_2 for Ls=332°, averaged over an area close to the south evening limb of the planet. This region was selected because it corresponded to the maximum CO_2 line depth, and thus insured a higher *S/N* than the region of maximum radiance. The best fit value of the H_2O_2 mixing ratio is 15 ppb. The water vapor abundance was retrieved from the 1236.295 cm^{-1} HDO transition, associated with the 1235.65 cm^{-1} line of CO_2. The best fit of the water vapor mixing ratio, in the selected area, was 150 ppm (Fig. 13).

Fig. 14 shows the TEXES and GCM maps corresponding to Ls=332° for hydrogen peroxide, water vapor and the surface temperature. In the case of H_2O_2 and H_2O, significant discrepancies appear between the observations and the GCM simulations. The measured abundances of both molecules are weaker than expected and their spatial distributions are very different. The TEXES H_2O_2 map exhibits a clear meridional stripe of lower intensity along the central meridian, which is not well reproduced by the model. In the case of H_2O, the discrepancy is even stronger in the spatial distributions. We believe that the TEXES H_2O map is reliable, because it was confirmed by another map retrieved from another HDO transition at 1239.95 cm^{-1}, also used during the 2003 run. In the case of the surface temperature, the agreement is better between the observations and the modeling, although some departure is present in the longitudes of the maximum flux, which appears at higher southern latitudes than expected from the GCM.

There is no clear explanation for this discrepancy. The presence of aerosols might be at least partially responsible for explaining the differences in the spatial distributions. It should be mentioned also that, since the publication of these results, the water cycle of the LMD GCM has been adjusted to agree better with the revised TES climatology showing water vapor columns reduced by ~30% (Lefèvre et al., 2008). Recent results obtained with this improved version of the model indicate lower H_2O and H_2O_2 amounts near equinox and are therefore in better agreement with TEXES data (see Sections 4.3.2, 5.1 and Fig. 16).

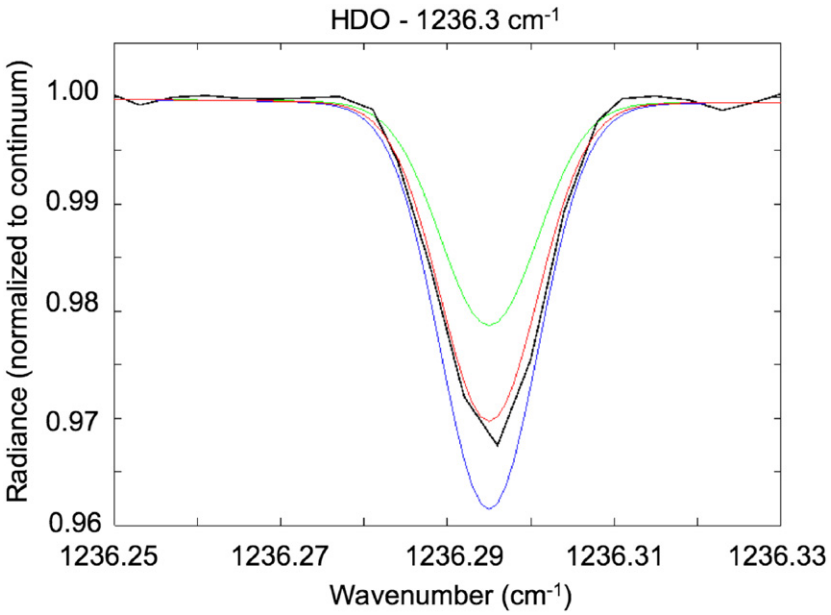

Fig. 13. The TEXES spectrum of HDO averaged over an area close to the southern evening limb (same as for Fig. 12), compared with synthetic models. Green: $[H_2O]=100$ ppm; red: $[H_2O]=150$ ppm; blue: $[H_2O]=200$ ppm. The figure is taken from Encrenaz et al. (2008). (For interpretation of the references to color in this figure legend, the reader is referred to the web version of this article.)

4.3.2. Ls=352° (October 2009)

Data were obtained between Oct. 11 and Oct. 15, 2009. The Doppler shift allowed us to use the 1239.995 cm^{-1} transition of HDO, as in the case of the 2003 data set. H_2O_2 was detected throught its 1241 cm^{-1} doublet.

Fig. 15 shows the retrieved maps of H_2O and H_2O_2, compared with the GCM simulations. The size of the Martian disk (6 arcsec) is small, and the expected amount of H_2O is weak, so the *S/N* is limited.

The mean mixing ratio of H_2O_2 is of the order of 15 ppb. This amount is well reproduced in Fig. 15 by an updated version of the LMD GCM, which produces less H_2O_2 at this season than previously published by Lefèvre et al. (2008). However, the measured spatial distribution does not show the large-scale minimum calculated by the model at high northern latitudes. It must be borne in mind that the TEXES H_2O_2 spatial distribution may not be significant because of the limited *S/N*, as illustrated by the artifact appearing on the right side of the map.

The low H_2O water content and its spatial distribution are in reasonable agreement with the GCM, with a maximum in the southern hemisphere and the morning limb. The mean mixing ratio of 100 ppm corresponds to a water vapor column density of approximately 6 pr-μm, as expected for this season.

The observed continuum map is in agreement with the simulation of the surface temperature distribution; however, the maximum observed value (260 K), calculated with a typical emissivity of 0.95, is lower than the GCM simulation (280 K). A surface emissivity of about 0.6 would be necessary to reconcile both values, which is unlikely. A more plausible explanation might come from the uncertainty of the TEXES absolute calibration.

5. The seasonal cycle of hydrogen peroxide

5.1. Comparison with the LMD GCM

Fig. 16 shows the observed seasonal variation of H_2O_2 on Mars, compared with the variation calculated at 20N and 20S by the updated version of the LMD GCM. Two simulations are considered, with and without the implementation of heterogeneous chemistry on water-ice clouds. These simulations produce a slightly smaller water vapor content than found by Lefèvre et al. (2008), which allows a better agreement with the TES and TEXES H_2O observations.

Data are from TEXES and from submillimeter observations from ground (Clancy et al., 2004) and space (Hartogh et al., 2010). The TEXES data correspond to mid-northern latitudes for Ls=0–180°, and to mid-southern latitudes for Ls=180–360°, in order to be more representative of the observing conditions induced by the axial tip of the planet. The submillimeter data are integrated over the whole disk.

It can be seen that heterogeneous chemistry on ice clouds makes no significant difference during the period Ls=180–360°. In contrast, between Ls=0 and 180°, the H_2O_2 abundance predicted by the GCM when heterogeneous chemistry is taken into account is significantly lower than the value predicted under the assumption of gas-phase only chemistry. TEXES data definitely favor this latter simulation, as already pointed out by Lefèvre et al. (2008). There is still a discrepancy between the GCM and the very low upper limit (2 ppb) derived with HERSCHEL/HIFI for Ls=77° (Hartogh et al., 2010). There is presently no explanation for this very low upper limit, which contradicts the TEXES measurement of 10 ppb obtained for Ls=80° two years before. One can wonder whether the discrepancy could be due to an inhomogeneous distribution of H_2O_2 at this season; however, as shown in Fig. 7, GCM simulations predict a maximum in the northern hemisphere, which was included in the Herschel field of view at the time of its observation (April 2010).

For the southern spring season (Ls=180–270°), the agreement between the observations and the models is quite satisfactory. Around the vernal equinox, the updated GCM, as compared with Lefèvre et al. (2008), gives a good agreement with the TEXES data, also visible in Fig. 15 (October 2009 data). A more general analysis of the whole H_2O_2 data set, using the updated GCM, is in preparation.

In summary, we now reach a good overall agreement, at least for the globally averaged H_2O_2 mixing ratio, for all seasons except

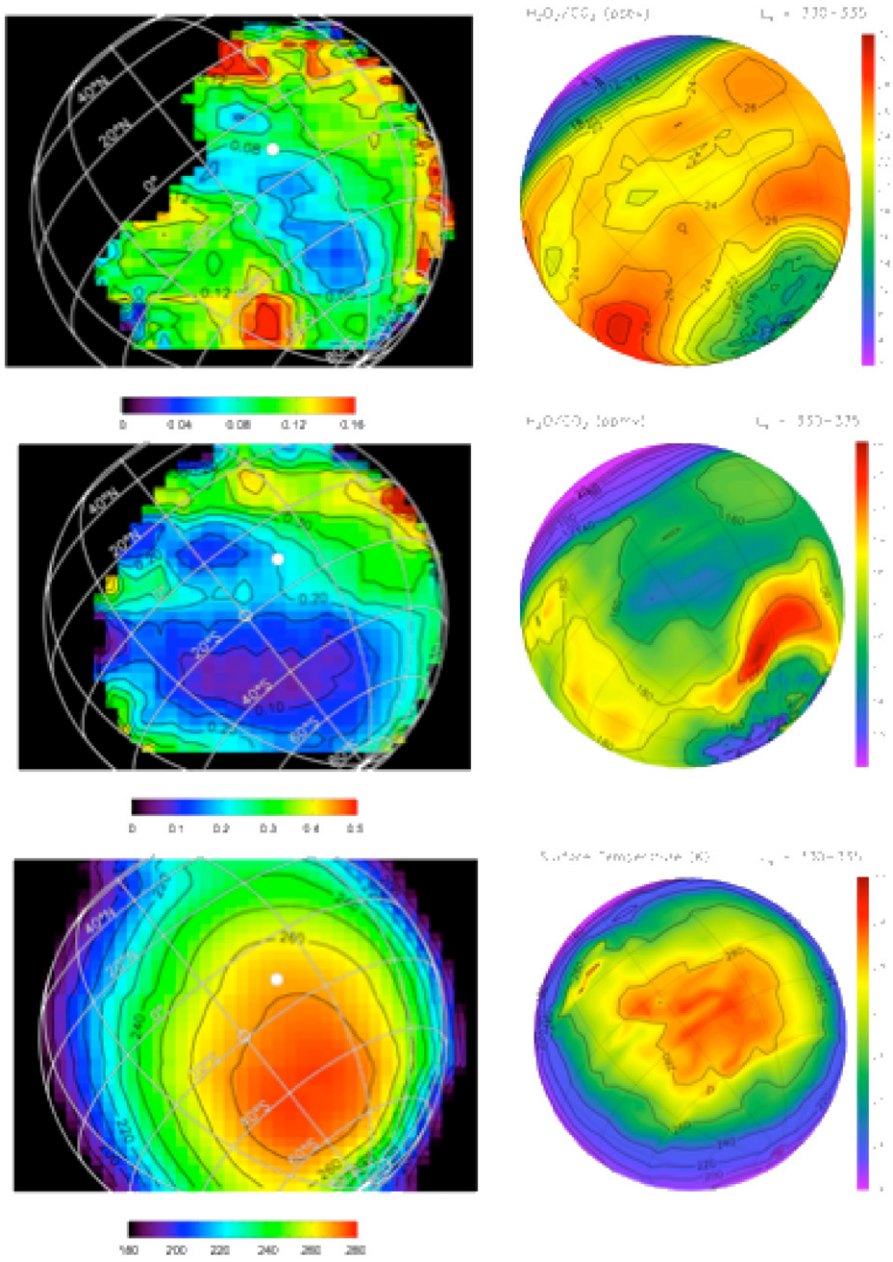

Fig. 14. Comparison of TEXES maps (left) and LMD GCM calculations (right) for the December 2005 data set (Ls=332°). Top: H_2O_2/CO_2 line depth ratio (left) and H_2O_2 mixing ratio (right; Green: 15 ppb). A line depth ratio of 0.13 (green area) corresponds to a H_2O_2 mixing ratio of 15 ppb. Middle: HDO/CO_2 line depth ratio (left) and H_2O mixing ratio (right; Green: 150 ppm); a line depth ratio of 0.3 (green area) corresponds to a water vapor mixing ratio of 150 ppm. Bottom: Surface temperatures: TEXES map, assuming an emissivity of 0.95 (left) and GCM map (right). The white dot on the TEXES map is the subsolar point. The figure is adapted from Encrenaz et al. (2008). (For interpretation of the references to color in this figure legend, the reader is referred to the web version of this article.)

around the northern summer solstice, when a strong discrepancy is still noted with the Herschel upper limit at Ls=77°.

5.2. Comparison with other simulations

Fig. 16 also shows the results of Moudden (2007) who used a GCM with on-line chemistry to calculate the evolution of H_2O_2 and water vapor as a function of the solar longitude. Results averaged over 5 sols are presented for Ls=0°, 90°, 180° and 270°. Values corresponding to latitudes of 0 (Ls=0° and 180°), 20N (Ls=90°) and 20S (Ls=270°) are indicated in Fig. 16. Moudden (2007) points out the important effect of condensation in the polar regions.

Also represented in Fig. 16 are the results of Krasnopolsky (2006, 2009) obtained with a 1D model assuming heterogeneous loss of H_2O_2 on water-ice particles. This differs from the GCM calculations of Lefèvre et al. (2008), which only included OH and HO_2 adsorption on ice without direct heterogeneous loss of H_2O_2. It can be seen that model results by Krasnopolsky (2009) tend to be in better agreement with the low upper limit inferred by Herschel/HIFI at Ls=77°. Unfortunately, there are no observational data available for Ls=120°–200°, where departures between models are greatest. Between 200° and 360°, both Krasnopolsky's model and the LMD GCM are in agreement with the observations. In conclusion, more data are necessary, especially at Ls=0°–200°, to better discriminate between the models.

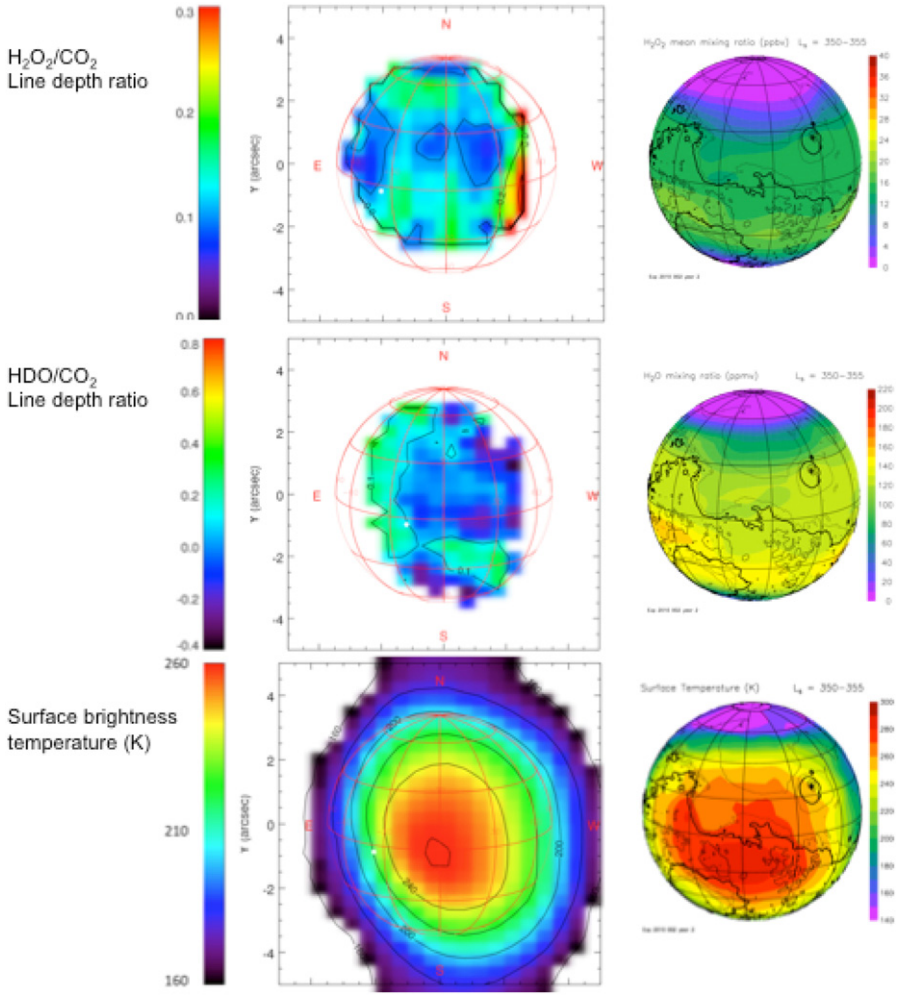

Fig. 15. Comparison of TEXES maps (left) and LMD GCM simulations (right) for the October 2009 data set (Ls=352°). Top: H_2O_2/CO_2 line depth ratio (left) and GCM map of the H_2O_2 mixing ratio (right); a line depth ratio of 0.13 corresponds to a mixing ratio of 15 ppb. The red spots on the right side of the TEXES map are attributed to artifacts. Middle: HDO/CO_2 line depth ratio (left) and the GCM map of the H_2O mixing ratio (right); a line depth ratio of 0.2 corresponds to a water vapor mixing ratio of 100 ppm. Bottom: Surface temperature. The TEXES surface temperature is calculated assuming a surface emissivity of 0.95. The white dot on the TEXES map is the subsolar point.

6. Detectability of localized H_2O_2 sources on Mars

6.1. Origin of localized H_2O_2 sources

The photochemical models mentioned above only consider photochemistry by solar radiation as a mechanism of hydrogen peroxide production on Mars. Recently, a new mechanism has been proposed, based on the production of large-scale electrostatic fields during dust storms and dust devils (Delory et al., 2006 and Atreya et al., 2006; 2007). The origin of these fields is believed to be triboelectric charging at the dust grain level, generated during collisions between dust-dust and dust–sand particles. Terrestrial analogs and simulations have shown that convective dust storms can separate charged grains resulting in a large-scale electrostatic dipole-like field, with a strength as high as 20 kV/m (Delory et al., 2006). Such electrostatic fields are capable of dissociating CO_2 and H_2O to form ion pairs of CO/O^- and OH/H^- following the reactions:

$$CO_2 + e \rightarrow CO + O^-$$

$$H_2O + e \rightarrow OH + H^-$$

Atreya et al. (2006, 2007) have developed a photochemical model, based on the model by Wong et al. (2003), which takes into account the above processes. They find that the production of OH by triboelectricity has a significant effect on subsequent neutral chemistry of the atmosphere. The additional OH production increases the production of hydrogen atoms which in turn increases the HO_2 production and hence the H_2O_2 production. The additional OH production also increases the destruction rates of HO_2 and H_2O_2 but to a much lesser extent, so that the net result is that the H_2O_2 production rate is increased by a factor as high as 10,000 compared to the classical values. The resulting mixing ratio could then reach 50–100 ppm. However, atmospheric temperatures of Mars are such that this H_2O_2 excess saturates and eventually precipitates out of the atmosphere, using silicate particles as condensation nuclei. For a surface temperature of 220 K – a mean value over seasons and latitudes – the H_2O_2 excess predicted by Atreya et al. (2007) in the presence of dust devils or dust storms may be 200 times the value inferred from classical photochemical models, i.e. about 4 ppm. So most of the H_2O_2 excess is adsorbed on aerosols and eventually bound in the regolith with a very long lifetime (from one hundred to several millions of years). Thus, in contrast to the gaseous H_2O_2, which has a lifetime of about 6 h, the hydrogen peroxide trapped on the soil could be a very efficient oxidizer, capable of scavenging any organic material present at the Martian surface.

We now estimate the maximum H_2O_2 gaseous content, which could be generated in dust devils or dust storms. Such events are expected to occur during southern spring and summer, close to

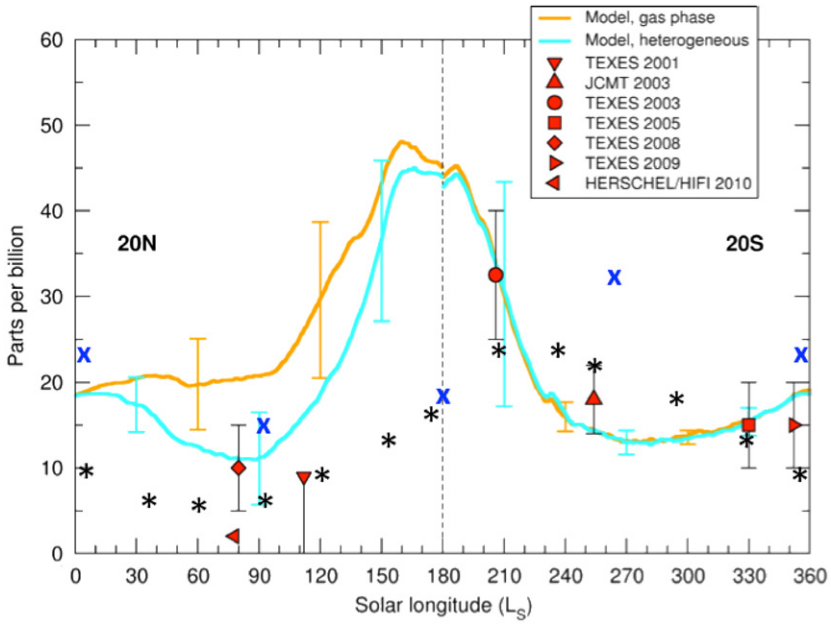

Fig. 16. The seasonal cycle of the H_2O_2 mixing ratio on Mars. TEXES observations refer to 20N latitudes for Ls=0–180° and to 20S latitudes for Ls=180–360°, in order to represent the observing conditions induced by the axial tip of the planet. Submillimeter observations refer to the entire disk. The LMD GCM simulations (yellow and blue curves), updated from the result of Lefèvre et al. (2008), ignore (yellow) or include (blue) heterogeneous chemistry. The Herschel point at Ls=77° corresponds to an upper limit. Other model simulations by Krasnopolsky (2009) and Moudden (2007) are represented by black stars and blue crosses, respectively. (For interpretation of the references to color in this figure legend, the reader is referred to the web version of this article.)

perihelion, when the surface temperature is at its maximum. As shown in Fig. 6, the maximum surface temperature may be above 300 K for this season. In this case, the saturation vapor curve of H_2O_2 could allow an enrichment of hydrogen peroxide corresponding to mixing ratios of a few ppm or even more, assuming of course that peroxide is not buried in the subsurface, which is actually a requirement for its longevity and subsequent removal of organics Concerning electrostatic fields, Kok and Renno (2009) point out that the effect of wind-blown sand, or saltation, which creates sand dunes and erodes geological features, could reduce the formation excess of hydrogen peroxide, because, according to these authors, electric discharges are expected to be less efficient in the presence of Martian saltation. On the other hand, a comprehensive plasma model indicates that it is the negatively charged dust, not sand, particles that are critical for producing large electrostatic fields up to 25 kV/m that extend to tens of km height (Farrell, 2009). Nevertheless, we recognize the controversy surrounding the effect of electrostatic fields on H_2O_2. In what follows, we analyze the detectability of a local H_2O_2 source corresponding to a typical mixing ratio of 1 ppm, considering this number as an upper limit only for the purpose of estimating its possible detectability.

In addition, we must remember that the source may be localized to small areas: the origin of a dust devil is typically less than a kilometer square at the Martian surface. In contrast, dust storms may develop over large areas and cover half an hemisphere or even the whole martian disk. On the other hand, the largest sustained electrostatic fields are expected be generated in the dust devils, in this case peroxide would be quite localized unless the aeolian boudaries shift over time. The enhanced peroxide abundance in the *atmosphere* is more likely to be seen only if the electrochemical process could be *caught in the act*, considering the extremely short lifetime of H_2O_2, which is further reduced by electrostatic fields, and the rapid dilution effect due to global mixing away from the source region.

6.2. Detectability of H_2O_2 sources

The best way to search for localized H_2O_2 sources consists in monitoring the southern hemisphere of Mars during southern spring. Three methods can be considered: ground-based infrared imaging spectroscopy with TEXES, infrared monitoring from Mars' orbit with the Planetary Fourier Spectrometer aboard Mars Express, and ground-based submillimeter interferometry with millimeter and submillimeters interferometers like IRAM (Institut de Radio-Astronomie Millimétrique) and later ALMA (Atacama Large Millimeter Array).

6.2.1. TEXES monitoring of H_2O_2 hot spots

Assuming an H_2O_2 mixing ratio of 1 ppm (i.e. 100 times our lower detectable limit which corresponds to H_2O_2 line depths of about 0.5%; see Fig. 7), for the maximum possible electrostatic fields, we expect H_2O_2 transitions of at least a few percent (depending upon the radiative transfer conditions), detectable in a few minutes. However, the typical spatial resolution of TEXES on the Martian disk is 1 arcsec (after apodization), which corresponds to a spot of 300 km at the surface. In the case of a dust devil, the dilution factor would thus be 10^5 so the event would not be detectable. The event might become detectable if it occurs over an area of at least 10 km in diameter, but the probability of such an event is very low, in view of the short H_2O_2 lifetime.

The observation would be made easier if TEXES were to be used on an 8-m class telescope like Gemini-N. In the future, the use of EXES (a slightly improved version of TEXES) aboard the SOFIA airborne observatory will allow the use of stronger transitions of the H_2O_2 ν_5 band, in the 1285–290 cm^{-1} range.

6.2.2. Search for H_2O_2 spots with PFS/Mars express

The ν_4 band of H_2O_2 exhibits strong transitions in the 350–400 cm^{-1} range. These transitions are not observable from the ground, because of nearby telluric absorptions by water vapor,

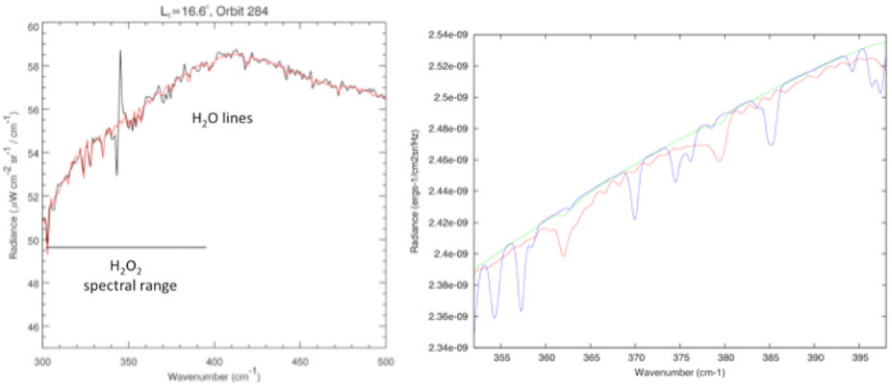

Fig. 17. Left : A spectrum of Mars between 300 and 500 cm^{-1}, integrated over one orbit, recorded by the Planetary Fourier Spectrometer. The spike at 350 cm^{-1} corresponds to an instrumental artifact. Absorption features are due to water vapor. The figure is taken from Fouchet et al. (2007). Right: Synthetic spectrum of Mars between 350 and 400 cm^{-1}. Models: H_2O=150 ppm (blue); H_2O_2=100 ppb (green) and H_2O_2=1 ppm (red). (For interpretation of the references to color in this figure legend, the reader is referred to the web version of this article.)

but they may be searched for on Mars using the Planetary Fourier Spectrometer aboard the Mars Express satellite (Fig. 17). PFS has the advantage of having a small field of view at pericenter (12 km for the Long-Wavelength Channel). The expected sensitivity per orbit (integrated over about 300 pixels) is in the range of 100 ppb at best. A mixing ratio of 2 ppm in one pixel could possibly be detectable with PFS. H_2O_2 transitions would have to be selected in spectral regions free from water contamination; this is the case, in particular, at 307, 343, 362 or 379 cm^{-1}. As shown in Fig. 17, for a mixing ratio of 1 ppm, the H_2O_2 signatures at 362 and 379 cm^{-1} are expected to be comparable in depth with the H_2O neighboring transitions. In any case, unless some exceptional transient event occurs, the detection of H_2O_2 with PFS is expected to be very challenging.

6.2.3. Search for H_2O_2 spots with submillimeter interferometry

Using submillimeter heterodyne spectroscopy with a 10-m single dish antennae, it is possible to reach an H_2O_2 limit of 20 ppb by integrating over the 10 arcsec diameter area (Clancy et al., 2004). If H_2O_2 spots of 1 ppm are present over a 1-arcsec area, they could be detectable with IRAM and, later, with ALMA (provided the observation takes place at the time of the transient event). With respect to IRAM, ALMA will have the triple advantage of a better seeing, and thus access to higher frequencies, a better sensitivity and a better spatial resolution.

7. Conclusions and perspectives

Observations of hydrogen peroxide over the past years have allowed monitoring of its seasonal behavior. The general trend of the observations is in reasonable agreement with the predictions of the photochemical models and, as for the ozone seasonal variations, seem to favor photochemical models including heterogeneous chemistry. However, there are still some discrepancies which remain to be understood. In particular, the recent Herschel measurement at Ls=77° (Hartogh et al., 2010) does not fit the other data nor the model predictions.

In the future, hydrogen peroxide on Mars should be detectable with the infrared spectrometer MATMOS aboard the ExoMars Trace Gas Orbiter (Wennberg et al., 2011). However, the best instrument to track localized H_2O_2 sources would be a submillimeter sounder in Mars' orbit. Such an instrument would combine a very high sensitivity, as illustrated by the Herschel measurement (Hartogh et al., 2010) and a high spatial resolution, as requested for detecting dust devils and dust storms. This instrument would be also ideal for monitoring the thermal structure up to high altitudes (up to 100 km) through the inversion of the CO lines; it would simultaneously retrieve the water vapor mixing ratio and the wind velocity fields. It is hoped that such an instrument will become be part of future orbiter payloads for monitoring the Martian aeronomy.

Acknowledgments

We wish to thank J. H. Lacy, M. J. Richter and the TEXES team for having designed and for operating the TEXES instrument, and the IRTF staff for operating the telescope. We are grateful to B. Bézard, T. Fouchet, F. Forget and S. Lebonnois for their help in the data analysis and interpretation. This research was funded by CNRS and INSU (Program National de Planétologie).

References

Atreya, S.K., Gu, Z.G., 1995. Photochemistry and stability of the atmosphere of Mars. Adv. Space Res. 16 (6), 57–68.
Atreya, S.K., Wong, A.S., Renno, N.O., Farrell, W.M., Delory, G.T., Sentman, D.D., Cummer, S.A., Marshall, J.R., Rafkin, C.R., Catling, D.C., 2006. Oxidant enhancement in Martian dust devils and storms: implication for life and habitability. Space Physics, Mars and Life, Astrobiology 6/3, 439–450 (special issue).
Atreya, S.K., Mahaffy, P., Wong, A.S., 2007. Methane and related trace species on Mars : origin, loss, implications for life, and habitability. Planet. Space Sci. 55, 358–369.
Atreya S.K., in press. The significance of trace constituents in the solar system, Faraday discussions. R. Soc. Chem. doi: 10.1039/c005460g.
Atreya, S.K., Witasse, O., Chevrier, V.F., Forget, F., Mahaffy, P.R., Price, B., Webster, C.R., Zurek, R.W., 2011. Methane on Mars: current observations, interpretation, and future plans. Special Issue on Methane on Mars, Planet. Space Sci. 59, 133–136.
Biemann, K., 1979. The implications and limitations of the findings of the Viking organic analysis experiment. J. Mol. Evol. 14, 65–70.
Biemann, K., Owen, T., Rushneck, D.R., La Fleur, A.L., Howarth, D.W., 1976. Search for organic and volatile inorganic components in two surface samples from the Chryse Planitia region of Mars. J. Geophys. Res. 82, 4641–4658.
Bjoraker, G. l., Mumma, M.J., Jennings, D.E., Wiedemann, G.R., 1987. An upper limit to the abundance of H_2O_2 in the Martian atmosphere. Bull. Am. Astron. Soc. 19, 818.
Clancy, R.T., Nair, H., 1996. Annual (aphelion–perihelion) cycles in the photochemical behavior of the global Mars atmosphere. J. Geophys. Res. 101, 12785–12790.
Clancy, R.T., Sandor, B.J., Moriarty-Schieven, G.H., 2004. A measurement of the 362 GHz absorption line of Mars atmospheric H_2O_2. Icarus 168, 116–121.
Delory, G.T., Farrell, W.M., Atreya, S.K., Renno, N.O., Wong, Ah-San, Cummer, S.A., et al., 2006. Oxidant enhancement in dust devils and storms: storm electric fields and electron dissociative attachment. Astrobiology 6, 451–462.
Encrenaz, T., Greathouse, T.K., Bézard, B., Atreya, S.K., Wong, A.S., Richter, M.J., Lacy, J.H., 2002. A stringent upper limit of the H_2O_2 abundance in the Martian atmosphere. Astron. Astrophys. 396, 1037–1044.

Encrenaz, T., Bézard, B., Greathouse, T.K., Richter, M.J., Lacy, J.H., Atreya, S.K., Wong, A.S., Lebonnois, S., Lefèvre, F., Forget, F., 2004. Hydrogen peroxide on Mars: evidence for spatial and temporal variations. Icarus 170, 424–429.

Encrenaz, T., Bézard, B., Owen, T., Lebonnois, S., Lefèvre, F., Greathouse, T.K., Richter, M., Lacy, J., Atreya, S., Wong, A.S., Forget, F., 2005. Infrared imaging spectroscopy of Mars: H_2O mapping and determination of CO_2 isotopic ratios. Icarus 79, 43–54.

Encrenaz, T., Greathouse, T.K., Richter, M.J., Bézard, B., Fouchet, T., Lefèvre, F., Montmessin, F., Forget, F., Lebonnois, S., Atreya, S.K., 2008. Simultaneous mapping of H_2O and H_2O_2 on Mars from high-resolution imaging spectroscopy. Icarus 195, 547–555.

Encrenaz, T., Greathouse, T.K., Bézard, B., Fouchet, T., Lefèvre, F., Montmessin, F., Bitner, M., Kruger, A., Richter, M.J., Lacy, J.H., Forget, F., Atreya, S.K., 2010. Water vapor map of Mars near summer solstice using ground-based infrared spectroscopy. Astron. Astrophys. 520, 33–38.

Farrell, W.M., 2009. Personal Communication.

Forget, F., Hourdin, F., Fournier, R., Hourdin, C., Talagrand, O., Collins, M., Lewis, S.R., Read, P., Huot, J.-P., 1999. Improved general circulation models of the Martian atmosphere from the surface and above 80 km. J. Geophys. Res. 104, 24155–24176.

Forget, F., Millour, E., Lebonnois, S., Montabone, L., Dassas, K., Lewis, S.R., Read, P.L., López-Valverde, M.A., González-Galindo, F., Montmessin, F., Lefèvre, F., Desjean, M.-C., Huot, J.-P., 2006. The new Mars climate database. In: Forget, F., Lopez-Valverde, M.A., Desjean, M.C., Huot, J.P., Lefevre, F., Lebonnois, S., Lewis, S.R., Millour, E., Read, P.L., Wilson, R.J. (Eds.), Proceedings of the Second Workshop on Mars Atmosphere Modelling and Observations, Granada, Spain, LMD, IAA, AOPP, CNES, ESA, February 27–March 3, 2006, p.128.

Fouchet, T., Lellouch, E., Ignatiev, N., Forget, F., Titov, D., Tschimmel, M., Montmessin, F., Formisano, V., Giuranna, M., Maturilli, A., Encrenaz, T., 2007. Martian water vapor : Mars Express PFS/LW observations. Icarus 190, 32–49.

Gough, R.V., Turley, J.J., Ferrell, G.R., Cordova, K.E., Wood, S.E., DeHaan, D.O., McKay, C.P., Toon, O.B., Tolbert, M.A., 2011. Can rapid loss, high variability of Martian methane be explained by surface H_2O_2? Planet. Space Sci. 59, 238–246.

Hartogh, P., Jarchow, C., Lellouch, E., de Vall-Borro, M., Rengel, M., et al., 2010. Herschel/HIFI observations of HCl, H_2O_2, and O_2 in the Martioan atmosphere—initial results. Astron. Astrophys. 521. doi:10.1051/0004-6361/201015160 idL49.

Hecht, M.H., Kounaves, S.P., Quinn, R.C., West, S.J., Young, S.M.M., Ming, D.W., Catling, D.C., Clark, B.C., Boynton, W.V., Hoffman, J., DeFlores, L.P., Gospodinova, K., Kapit, J., Smith, P.H., 2009. Detection of perchlorate and the soluble chemistry of martian soil at the phoenix lander site. Science 325, 64–67.

Huguenin, R.L., 1982. Chemical weathering and the Viking biology experiments on Mars. J. Geophys. Res. 87, 10069–10082.

Hunten, D., 1979. Possible oxidant sources in the atmosphere and surface of Mars. J. Mol. Evol. 14, 71–78.

Jacquinet-Husson, N., et al., 2005. The 2003 edition of the GEISA/IASI spectroscopic database. J. Quant. Spectr. Rad. Transfer 95, 429–467.

Klein, H.P., Horowitz, N.H., Biemann, K., 1992. The search for extant life on Mars. In: Kieffer, H.H. (Ed.), Mars. University of Arizona Press, Tucson.

Kok, J.F., Renno, N.O., 2009. Electrification of wind-blown sand on Mars and its implication for atmospheric chemistry. Geophys. Res. Letters 36, L05202.

Krasnopolsky, V.A., 1986. Photochemistry of the Atmospheres of Mars and Venus. Springer-Verlag, Berlin.

Krasnopolsky, V.A., 1993. Photochemistry of the Martian atmosphere (mean conditions). Icarus 101, 313–332.

Krasnopolsky, V.A., 1995. Uniqueness of a solution of a steady-state photochemical problem: application to Mars. J. Chem. Phys. 100, 3263–3276.

Krasnopolsky, V.A., 2006. Photochemistry of the Martian atmosphere: seasonal, latitudinal, and diurnal variations. Icarus 185, 157–170.

Krasnopolsky, V.A., 2009. Seasonal variations of photochemical tracers at low and middle latitudes on Mars: observations and models. Icarus 201, 564–569.

Krasnopolsky, V.A., Bjoraker, G.L., Mumma, M.J., Jennings, D.E., 1997. High-resolution spectroscopy of Mars at 3.7 and 8 μm: a sensitive search for H_2O_2, H_2CO, HCl, and CH_4, and detection of HDO. J. Geophys. Res. 102 (6525), 6534.

Lacy, J.H., Richter, M.J., Greathouse, T.K., Jaffe, D.T., Zhu, Q., 2002. TEXES: a sensitive high-resolution grating spectrograph for the mid-infrared. Pub. Astron. Soc. Pac. 114, 153–168.

Lefèvre, F., Lebonnois, S., Montmessin, F., Forget, F., 2004. Three-dimensional modeling of ozone on Mars. J. Geophys. Res. 109, E07004. doi:10.1029/2004JE002268.

Lefèvre, F., Bertaux, J.-L., Clancy, R.T., Encrenaz, T., Fast, K., Forget, F., et al., 2008. Heterogeneous chemistry in the atmosphere of Mars. Nature 454, 971–975.

Mancinelli, R.L., 1989. Peroxides and the survivability of microorganisms on the surface of Mars. Adv. Space Res. 9, 191–195.

Montmessin, F., Fouchet, T., Forget, F., 2005. Modeling the annual cycle of HDO in the Martian atmosphere. J. Geophys. Res. 110 (E3) (CiteID03006).

Moudden, Y., 2007. Simulated seasonal variations of hydrogen peroxide in the atmosphere of Mars. Planet. Space Sci. 55, 2137–2143.

Mumma, M.J., Novak, R.E., DiSanti, M.A., Bonev, B., dello Russo, N., Magee-Sauer, K., 2003. Seasonal mapping of HDO and H_2O in the Martian atmosphere. In: Proceedings of the Sixth International Conference on Mars, July 20–25, 2003, Pasadena, CA, abstract 3186.

Nair, H., Allen, M., Anbar, D., Yung, Y.L., Clancy, R.T., 1994. A photochemical model of the Martian atmosphere. Icarus 111, 124–150.

Navarro-González, R., Vargas, E., de la Rosa, R., Raga A.C., and McKay, C.P., in press. Reanalysis of the Viking results suggests perchlorate and organics at 5 mid-latitudes on Mars. J. Geophys. Res.

Novak, R.E., Mumma, M.J., Villanueva, G., DiSanti, M.A., Bonev, B., Rahon, C.L., Sanstead, C.C., 2007. Seasonal mapping of HDO/H_2O in the Martian atmosphere. Bull. Am. Astron. Soc. 39, 455.

Oyama, V.I., Berdahl, B.J., 1977. The Viking gas exchange experiment results from Chryse and Utoplia surface samples. J. Geophys. Res. 82, 4669–4676.

Parkinson, T.D., Hunten, D.M., 1972. Spectroscopy and aeronomy of O_2 on Mars. J. Atmos. Sci. 29, 1380–1390.

Quinn, R.C., Zent, A.P., 1999. Peroxide-modified titanium dioxide: a chemical analog of putative Martian soil oxidants. Orig. Life Evol. Biosphere 29 (1), 59–72.

Rohlfs, K., Wilson, T.L., 2004. Tools of Radio Astronomy. Springer-Verlag, Berlin.

Rothman, L.S., 1986. Infrared energy levels and intensities of carbon dioxide, Part 3. Appl. Opt. 25, 1795–1816.

Wennberg, P.O., Hipkin, V.J., Drummond, J.R., Dalhousie, U., Toon, G.C., Allen, M., et al., 2011. MATMOS: the Mars atmospheric trace molecule occultation spectrometer. In: Proceedings of the Fourth International Workshop on the Mars Atmosphere : Modelling and Observations, Paris, February 8–11, 2011.

Wong, A.S., Atreya, S.K., Encrenaz, T., 2003. Chemical markers of possible hot spots on Mars. J. Geophys. Res. 108 (E4). doi:10.1029/2002JE002003 CiteID 5026.